Nano Energy 47 (2018) 401–409

Contents lists available at ScienceDirect

Nano Energy

journal homepage: www.elsevier.com/locate/nanoen

Full paper

Understanding and modeling of triboelectric-electret nanogenerator

Ronan Hinchet[a], Ali Ghaffarinejad[b,c], Yingxian Lu[b], Javad Yavand Hasani[c], Sang-Woo Kim[a,*], Philippe Basset[b,*]

[a] School of Advanced Materials Science and Engineering, Sungkyunkwan University (SKKU), Suwon, 440-746, Republic of Korea
[b] Université Paris-Est, ESYCOM, ESIEE Paris, Noisy-le-Grand 93162, France
[c] School of Electrical Engineering, Iran University of Science and Technology, Tehran 16846-13114, Iran

ARTICLE INFO

Keywords:
Triboelectric nanogenerator
Kinetic energy harvester
Triboelectric generator simulation
Triboelectric-electret (triboelectret) nanogenerator
T-ENG

ABSTRACT

Recently, electrostatic kinetic energy harvesters regained strong attention through the development of new triboelectric generators for harvesting green and renewable energy. These devices use a triboelectric dielectric layer as electret for polarizing their capacitance and they behave similarly to electret generators. However, triboelectric-based electret nanogenerators (T-ENG) have specificities arising from the contact electrification phenomenon and leading to different performances. For better understanding T-ENG, we investigated their electrical modeling with lumped-elements and multiphysics simulation in light of last researches on electret generators. To take into account T-ENG specificities, we experimentally measured the amplitude of the triboelectric effect on perfluoroalkoxy alkane films. This approach allowed fully simulating T-ENG and the model was found in agreement with experimental results. Understanding and verifying the model is capital, but to go further toward the application of T-ENG, we reused two electret circuits to extract the T-ENG model parameters in view of facilitating their realistic modeling and practical development into application.

1. Introduction

With the growth of microsystems and the need to make them autonomous, the research on energy-harvesting systems remarkably increased and accelerated recently, especially for electrostatic kinetic energy harvesters (e-KEH). These devices use an electrostatic field in a variable capacitance to convert mechanical energy into electricity. The electrostatic field polarizing the variable capacitance is generated using a direct current voltage source (electret-free devices), or using an electret layer inserted into the variable capacitance (electret-based devices). Electrostatic electret generators appeared in 1978 [1] and their basis and theory were introduced in 1992 [2]. Early investigations in 1987 [3] concluded on the apparent superiority of e-beam and corona discharge techniques to trap charges in a dielectric and to induce a strong electric field in view of harvesting mechanical energy and sensing. At that time triboelectricity was left aside. However, in 2012 triboelectric-based electret generator, commonly called TENG for triboelectric nanogenerator, started to be investigated by Fan et al. [4] in light of last progresses made in nano electro mechanical systems and especially in nano piezoelectricity. It is now the subject of a lot of attention as it could contribute to solve some modern energy issues.

As for other electret generators, TENGs also belong to the family of electrostatic kinetic energy harvesters (e-KEH). Electrets are dielectric materials that are in an electric polarization state [5], like an electrical equivalent of a magnet [6–9]. They can be made by charge injection in a dielectric (ionic or electronic implantation [10–12] or by dipole orientation of ferroelectric materials [13] like poly(vinylidenefluoride-*co*-trifluoroethylene)) [14]. Charged-based electret generators can be divided into two categories: first the permanent (or quasi permanent) electrets where charges remain for a few months to tens of years [15]. They are usually made by injecting charges more or less deeply [16,17] in a dielectric layer using various processes like corona discharge [18], e-beam [19], photo excitation, X-ray or thermal excitation for instance [3,20,21]. Secondly, the temporary electrets where charges can remain from few minutes to few days. They are generated on the surface of a dielectric by mechanical contact or friction also called triboelectrification. In all electret generators, the way to charge the electret layer and the location of the charges in the electret layer may differ. However, they all convert mechanical movements, like vertical [22] and lateral vibrations [23], translations [24] or rotations [25], into electrical energy using the same physic and principle of e-KEH [7]. Therefore, they follow the same constitutive equations and model.

In this paper, we investigate the constitutive equations, the lumped-element modeling and the finite element method (FEM) multiphysics simulation of triboelectric-based electret nanogenerators (T-ENG) in light of the extensive literature of e-KEH. We explain the main

* Corresponding authors.
E-mail addresses: kimsw1@skku.edu (S.-W. Kim), philippe.basset@esiee.fr (P. Basset).

https://doi.org/10.1016/j.nanoen.2018.02.030
Received 23 January 2018; Received in revised form 13 February 2018; Accepted 14 February 2018
Available online 21 February 2018

equations governing the electrical model of T-ENG and we compare our result with FEM multiphysics simulations. Experimentally we approach the triboelectric charge generation and compare experimental results with our model. Last, we propose simple setups allowing to extract experimentally the main T-ENG model parameters and to evaluate its performance. This will be very useful for a better understanding of T-ENGs and for developing and integrating T-ENG in industrial and consumer electronics.

2. Methods

2.1. Modeling and simulations

Electrical lumped-parameter modeling have been computed using LTspice and FEM simulations have been performed using COMSOL Multiphysics.

2.2. Experimental characterization

Surface voltage measurements have been performed using an electrostatic voltmeter Trek 347. A low frequency generator coupled with an inertial shaker (Mini SmartShaker K2007E01 from The Modal Shop (TMS)) was used to actuate the T-ENG. The output voltages generated by the T-ENG have been measured using oscilloscope and high impedance follower circuit setups.

3. Theory and modeling

E-KEHs, and so T-ENGs, are based on a variable capacitive structure made up generally of two (or more) electrodes separated by a dielectric that is typically air (or vacuum). An electret, made of a solid dielectric layer, can be inserted between the capacitance's electrodes. Depending on the electret fabrication process, charges are injected on the surface or deeper inside the dielectric layer. It is generally assumed that for corona discharge, charges are concentrated close to the surface of the electret and therefore there are assimilated to a surface charge distribution characterized by its surface charge density σ. For contact electrification, the triboelectric charges are located on the surface, within a thickness even smaller (tens of nm) than that in corona charging. However, for e-beam or X-ray charging for example, charges can be deeply implanted at tens of μm [17] and distributed in the depth of the electret. In these cases, a "virtual" surface charge density can be approached by integrating the depth distribution profile of the volume charge density ρ over the depth [6]. Here, we considered an electret created by contact electrification that we call triboelectret. It has a surface S, a triboelectric dielectric layer thickness d_{die}, a permittivity ε_{die}, a total triboelectric charge Q_{TE} and a triboelectric charge density σ_{TE}; deposited on the bottom electrode and facing the moving top electrode with a variable air gap d_{var} and permittivity ε_{air} (Fig. 1a).

As described in electret's literature [6–9,21], Triboelectret devices are governed by electrostatic laws. By applying the Kirchhoff's law and the Gauss's law, we have:

$$E_{die} d_{die} + E_{var} d_{var} = 0 \quad (1)$$

$$E_{die} \varepsilon_{die} - E_{var} \varepsilon_{air} = Q_{TE}/S = \sigma_{TE} \quad (2)$$

where E_{var} and E_{die} are the electric fields in the air gap and the triboelectret respectively. By solving these equations, we have:

$$E_{die} d_{die} = \frac{\sigma_{TE} d_{die}}{\varepsilon_{die}\left(1+\frac{\varepsilon_{air} d_{die}}{\varepsilon_{die} d_{var}}\right)} \quad (3)$$

Here $E_{die} \times d_{die}$ represents the voltage at the surface of the triboelectric layer V_{TE}, often called V_{bias} especially in non-triboelectric e-KEH. It can be measured using an electrostatic probe [26] such as an electrostatic voltmeter if the two electrodes of the T-ENG can be easily separated. V_{TE} depends on the triboelectric charge distribution σ_{TE} on the top of triboelectret layer, the permittivity of the layers and their thicknesses. If the triboelectric layer is much thinner than the air gap ($d_{var} > > d_{die}$), V_{TE} can be approached by:

$$V_{TE} \approx \sigma_{TE} d_{die}/\varepsilon_{die} = Q_{TE}/C_{die} \quad (4)$$

where C_{die} is the capacitance of the triboelectric dielectric layer. Consequently, V_{TE} polarizes the device and charges its capacitance. When a relative movement occurs between the two electrodes, the device's capacitance varies. As a result, the charges are reorganized, moving through the external resistive load Z, therefore inducing a current.

The T-ENG structure is composed of a fixed capacitor and a variable capacitor in series (Fig. 1b). The variable capacitor consists of the top electrode, the air gap and the charged top surface of the triboelectret layer. The fixed capacitor is composed of the same surface charge, the triboelectret dielectric layer and the bottom electrode. After the initialization of the device, i.e. the charge injection or the contact electrification of the triboelectret layer, the device is considered electrically neutral. This hypothesis of neutrality is essential for electrical analysis of the T-ENG. Because the system is neutral at any time due to the law of charge conservation, the sum of the charges in the electrodes Q_{var} and Q_{die}, and the charge of the triboelectret layer generated by contact electrification Q_{TE} is null [7]:

$$Q_{TE} + Q_{var} + Q_{die} = 0 \quad (5)$$

It is important to note that Q_{var} and Q_{die} are unknown and depend on the position of the top electrode that is varying with the time t, the charge of the triboelectret Q_{TE} and the load Z. However, using Eqs. (1)–(5) and the Poisson's equation, it is possible to approach the voltage generated by such T-ENG:

$$V_{T-ENG} = -\int_0^{d_{die}} E_{die} dx - \int_{d_{die}}^{d_{die}+d_{var}} -E_{var} dx = -E_{die} d_{die} + E_{var} d_{var} \quad (6)$$

$$V_{T-ENG} = -\frac{Q_{die} d_{die}}{S \varepsilon_{die}} + \frac{Q_{var} d_{var}}{S \varepsilon_{air}} \quad (7)$$

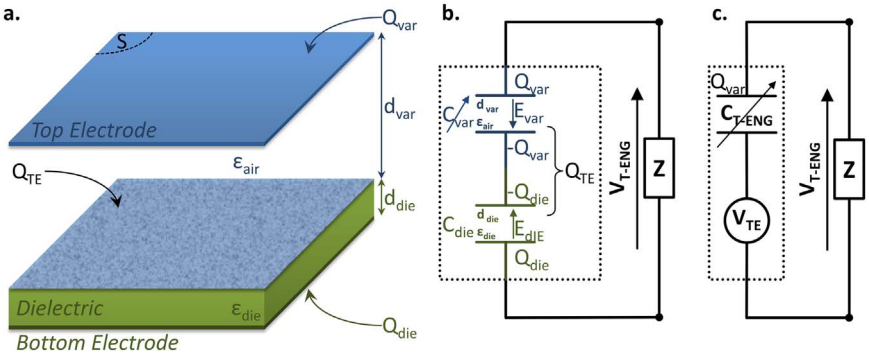

Fig. 1. T-ENG electrical model. a. Schematic of the T-ENG in the vertical contact configuration. The T-ENG has a surface S. The total charge in the top and bottom electrodes is Q_{var} and Q_{die} respectively. The dielectric electret layer has a thickness d_{die} and a permittivity ε_{die}. It has a top total triboelectric surface charge Q_{TE}. The air gap between the electret and the top electrode has an initial thickness d_{var} and a permittivity ε_{air}. b. Detailed electrical model of the T-ENG and parameters. c. Compact electrical model of the T-ENG [7].

$$V_{T-ENG} = \frac{Q_{TE} d_{die}}{S\varepsilon_{die}} + \frac{Q_{var}}{S}\left(\frac{d_{die}}{\varepsilon_{die}} + \frac{d_{var}}{\varepsilon_{\text{air}}}\right) \quad (8)$$

Eq. (7) has two parts; each of them implying a voltage drop across a capacitor. The first part is associated to C_{die}, which is equal to (Fig. 1b):

$$C_{die} = \frac{S\varepsilon_{die}}{d_{die}} \quad (9)$$

The second part is associated to the total capacitance of the device $C_{T\text{-}ENG}$:

$$C_{T-ENG} = \frac{C_{var} C_{die}}{C_{var} + C_{die}} = S\frac{1}{\frac{d_{die}}{\varepsilon_{die}} + \frac{d_{var}}{\varepsilon_{\text{air}}}} \quad (10)$$

By substituting these terms into Eq. (8), we can express the voltage of the T-ENG as:

$$V_{T-ENG} = \frac{Q_{TE}}{C_{die}} + \frac{Q_{var}}{C_{T-ENG}} = V_{TE} + \frac{Q_{var}}{C_{T-ENG}} \quad (11)$$

In stationary regime Q_{TE} is constant, and therefore V_{TE} represents the constant voltage source generated by contact electrification and is equivalent to the one obtained by corona discharge. It is important to note that V_{TE} only depends on the triboelectric charge and the thickness of the triboelectric layer, not on the air gap if it is much bigger than the thickness of the triboelectret ($d_{var} >> d_{die}$) [27–29]. Therefore, triboelectric and electret generators share the same electric model: a constant voltage source, which the value is equal to the surface voltage of the triboelectret V_{TE}, in series with the variable capacitance of the T-ENG ($C_{T\text{-}ENG}$) (Fig. 1c) [8].

4. Calculations and simulations

The current and voltage generated by the T-ENG depend on both the characteristics of the electromechanical transducer (position of the mobile electrode, charge of the triboelectret, etc.) and its conditioning circuit that can be a simple resistance or a more complex circuit. For a T-ENG connected to a resistive load Z, the Kirchhoff's law give the equation of the voltage in the circuit [6–8]:

$$Z \times \frac{dQ_{var}(t)}{dt} + \frac{Q_{var}(t)}{C_{T-ENG}(t)} = V_{TE} \quad (12)$$

This differential equation with time variable coefficients cannot be fully solved analytically. Blokhina et al. [30] studied this problem and concluded that this equation does not have a closed form solution because the analytical solution of $Q_{var}(t)$ can only be an infinite (Fourier) series. However as explained by Galayko et al. [31], the terms above the third or fourth can be neglected in most practical cases, which simplify the problem, but the coefficients of the series are expressed through Bessel functions, which make them more difficult to find. Some approximations [29,32] and simplifying assumptions [25,33] have been used to approach a solution under certain vibration excitations. This approach allowed to estimate analytically the maximum power generated [34,35], which can be of great help for optimizing electret energy harvesters [31]. Nevertheless, these equations can be resolved numerically using a Spice software or Simulink for example [36–39]. This gives access to numerous parameters and values of the system while being much more precise and exact.

Based on the established description of the electret generators in the literature and the analogy with T-ENGs, we simulated a vertical contact T-ENG. For comparison and to verify our model, we first used the same geometrical and material parameters used in recent papers published on the modeling and simulation of T-ENGs [27–29] (Table 1).

Our simulation results showed exactly the same voltage and current profile that in [27–29] during the first capacitance variation. Then we push our model further and analyzed the device over multiple cycles. As expected by such electrical circuits including resistances and capacitors, we found that our T-ENG model has first a transitory regime and then reaches a stationary regime. We found that the transitory regime is very sensitive to the model parameters and the initial conditions such as the top electrode position (Fig. 2a). Under $Z = 100\ \text{M}\Omega$ and for electrode's contact as initial position ($\varphi = 0$), it took half a period to reach the stationary regime (Fig. 2b). When increasing the load resistance, it can take up to 1200 cycles (4 min) for $Z = 1\ \text{T}\Omega$ for example (Fig. 2c). This transitory regime can be adjusted by changing judiciously the initial position of the top electrode, from the closed gap ($\varphi = 0$) to a position at the middle of the maximum gap ($\varphi = \pi/2$) (Fig. 2a). In this latter case, at $Z = 1\ \text{T}\Omega$, it takes only one cycle to reach the stationary regime and the difference between both regimes is small (Fig. 2c). Another method would be to solve the boundary condition $Q_{var}(t = 0) = Q_{var}(t = \text{T})$ to find the stationary regime [40].

Table 1
T-ENG parameters used for the electrical model simulation and comparison with [27].

T-ENG device and material parameters	
Dielectric (PTFE)	$\varepsilon_{rdie} = 3.4$ $d_{die} = 125\ \mu\text{m}$
Surface	$S = 0.005\ \text{m}^2$
Surface charge density	$\sigma_{TE} = -8\ \mu\text{C m}^{-2}$
Maximum gap	$x_{max} = d_{var} = 0.002\ \text{m}$
Velocity	$v = 0.1\ \text{ms}^{-1}$
Gap	$x = \frac{x_{max}}{2} - \frac{x_{max}}{2} \times \cos\left(\frac{\pi v}{x_{max}} t + \varphi\right)$
Gap movement phase	$\varphi = 0\ \text{rad}$
Load resistance	$Z = 100\ \text{M}\Omega$

This change of regime can have a dramatic impact on the T-ENG performance expectations, and has to be taken into account. Thereby, simulating and considering only the transitory regime, we can expect that the T-ENG will generate up to 304 V and 3.04 μA peaks at $Z = 100\ \text{M}\Omega$, and a maximum (instantaneous) power $P_{max} = 1.11$ mW at the optimum impedance of $Z_{opt} = 315\ \text{M}\Omega$. However, these values are actually largely over-estimated (Fig. 2d). During the stationary regime, the T-ENG generates only 38.7 V and 387 nA peaks at $Z = 100\ \text{M}\Omega$, corresponding to a maximum (instantaneous) power $P_{max} = 194\ \mu\text{W}$ at $Z_{opt} = 2\ \text{M}\Omega$, which is much lower. To get a correct representation of the power generation ability of the T-ENG, we also calculated the root mean square (RMS) voltage and current generated, as well as the average power. They represent the equivalent continuous voltage, current and useful power generated by the T-ENG respectively, which allow a fair, full and better comparison of device performances independently of peak shapes and values. In addition, they also provide the values that are the most interesting from the perspective of engineering and practical applications, i.e. the stable output power we can really count on. The RMS voltage drop from 127 V in the transitory regime to 20.6 V in the stationary regime, and the RMS current drop from 1.27 μA to 206 nA at $R_L = 100\ \text{M}\Omega$. As for the average power that drops from 318 μW to 16.2 μW (Fig. 2d), which is 20 times lower. Finally, we observed a big shift of the maximum average power optimum impedance from 630 MΩ in the transitory regime to 3.6 MΩ in the stationary regime. It is also interesting to note that the impedance giving the maximum power peak is not the same but lower than the impedance giving the maximum average power. T-ENG devices should be designed according to this average values in stationary regime.

To verify our results and confirm our observations, we also performed time-dependent multiphysics simulations of the T-ENG using FEM. We chose smaller geometric parameters in order to have faster simulations (Table 2). From the 3D structure of the T-ENG (Fig. S2), we used mechanical equations to determine the position of the top electrode according to the time. We also included the electrostatic physic to add triboelectric charges and to compute the electric field, and we added the external electrical circuit composed of a resistive load of 100 MΩ. Finally, we performed time dependent simulations during 1 s (5 periods). Results show the electric potential distribution depending on time (Fig. 3a) and the voltage difference generated across the load

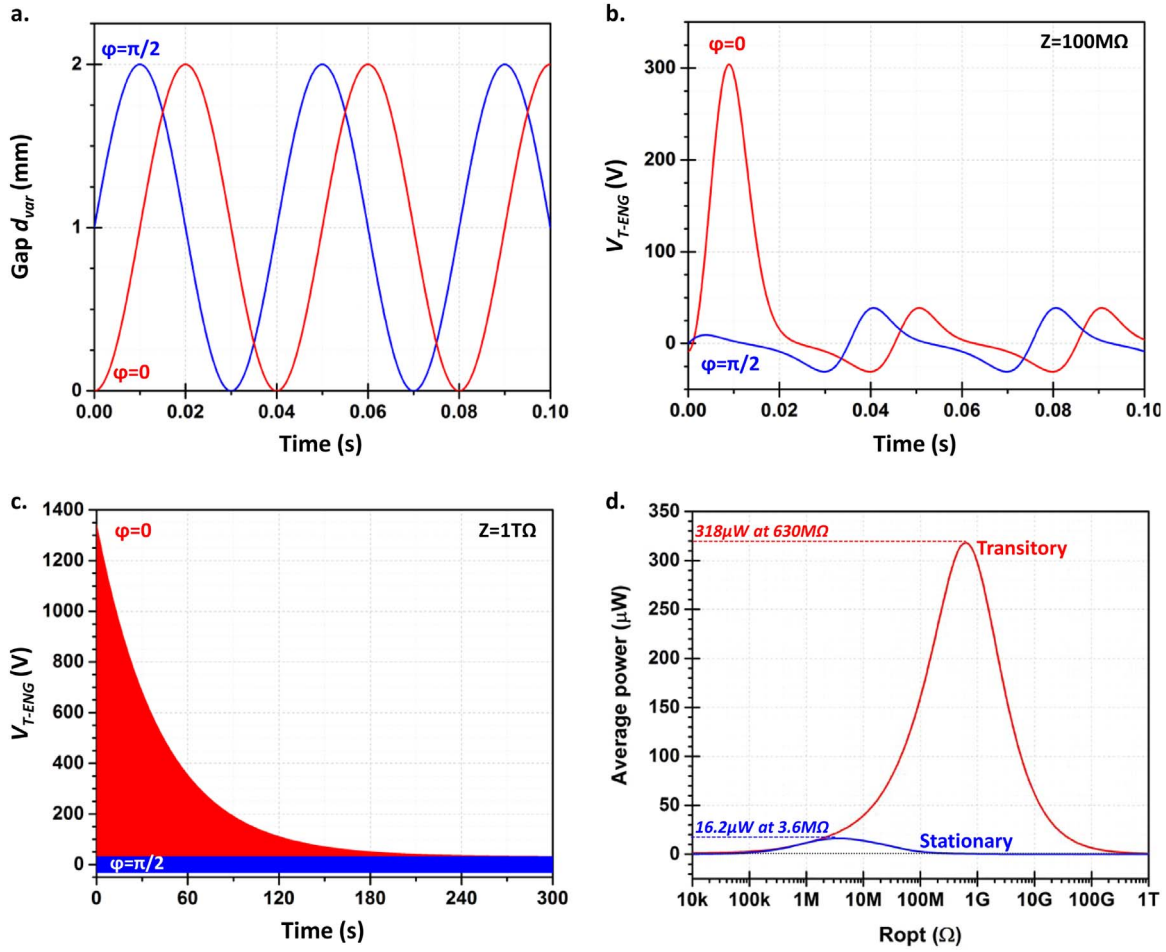

Fig. 2. Electrical model simulation results and comparison between the transitory and stationary regimes. a. T-ENG gap distance, b. electrode voltage difference under a resistance load of 100 MΩ and c. electrode voltage difference under a resistance load of 1 TΩ as a function of time and depending on the initial sinusoidal movement phase ϕ. d. Average power generated as a function of the resistance load during the first period of the transitory regime and during the stationary regime.

Table 2
T-ENG parameters used for the FEM simulation. They include a minimum gap and a frequency parameter.

FEM vertical contact mode T-ENG parameters	
Dielectric 1 (PFA)	$\varepsilon_{rdie} = 2.1$ $d_{die} = 50$ μm
Surface charge density	$\sigma_{TE} = -10$ μC m^{-2}
Maximum gap	$x_{max} = 1$ mm
Minimum gap	$x_{min} = 1$ μm
Surface	S = 0.0001 m^2
Frequency	f = 5 Hz
Load resistance	Z = 100 MΩ
Gap	$x = x_{min} + \frac{x_{max} - x_{min}}{2}(\sin(2\pi ft)+1)$

resistance *Z*. We also simulated with a Spice simulator the same T-ENG using the electrical model shown in Fig. 1c and we found very similar results (Fig. 3b). They agree very well and we only noted a tiny difference of less than 3%, which supports and strengthen the quality of the models.

For a better understanding of the T-ENG behavior, we plotted the charge-voltage (Q-V) [41,42] and the voltage-gap cycles (Fig. 3c and d). Because of the iterative computation and the convergence error method used by the FEM simulation, we observe that it generates cycles that converge progressively toward the electrical model, and reach a very good accuracy after a few cycles. The Q-V cycles turn clockwise. This indicates the creation of energy; therefore, the device is an energy generator [7]. The Q-V cycle area indicates that the device generates 5.5 nJ per cycle. The voltage-gap cycle shows that most of the voltage signal generated by the T-ENG occurs at a relatively small gap, less than 200 μm from the triboelectret layer, and beyond this distance, the signal is negligible. This is related to the capacitance change that mostly varies at short gap from 34 pF in contact to 4 pF at 200 μm. Then, once the capacitance of the device reaches a value of the same order than the parasitic capacitance of the circuit, there is no interest in an additional increase of the gap. In other words, above a certain gap it may be more interesting to stack multiple small devices rather than having a tall one. This is due to the nature of the electrostatic force induced by triboelectric electrostatic charges (electrets) and that is, for this contact-separate device geometry, reversely proportional to the square of the distance between the electrodes. It illustrates that, as explained in [7,8], electrostatic energy harvesters are most efficient at micro scale and does not scale up very well at macro scale, especially compared to other technologies available. The precise impact of parasitic capacitances on e-KEH have been detailed in [37,43,44].

5. Experimental results and discussion

To model precisely these T-ENGs, we must look closer to what make their specificity, *i.e.* the contact electrification that induces triboelectric charges on the surface of the dielectric layer. To go further than the simple consideration of an arbitrary triboelectric surface charge density and to get a better idea of its magnitude compared to corona charged electrets, we experimentally measured the surface voltage of triboelectric layers after rubbing and pressing, and we evaluated the

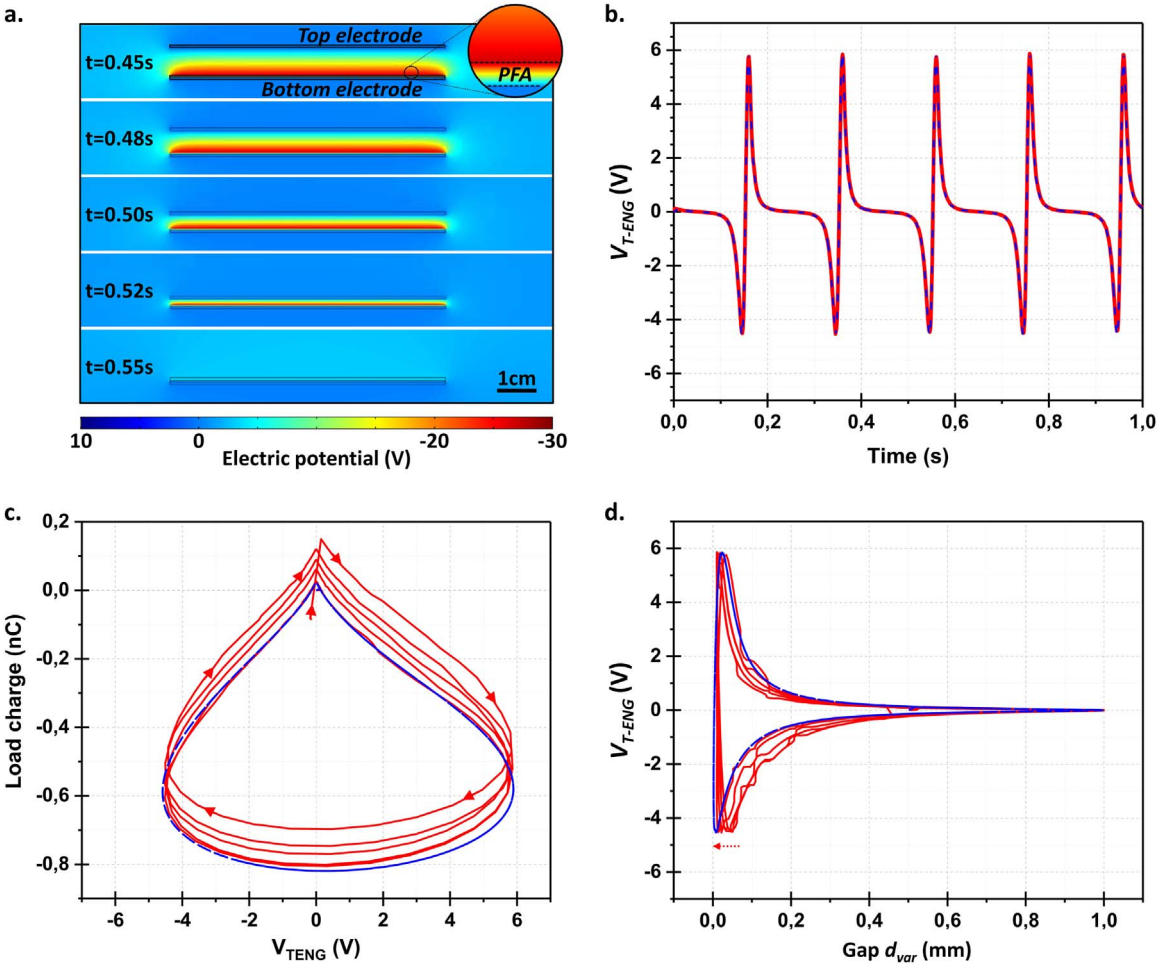

Fig. 3. FEM simulations results and comparison with the electric model. a. Electrostatic potential distribution at the middle of the T-ENG (XZ plan) at different time and computed by time dependent FEM simulation including the mechanical, electrostatic and electrical circuit physics. b. Comparison of the T-ENG electrodes potential difference computed by FEM simulation (red) and Spice electrical modeling (blue). c. T-ENG charge to voltage cycle and d. voltage cycle depending on the gap plotted for the FEM simulation and electrical modeling.

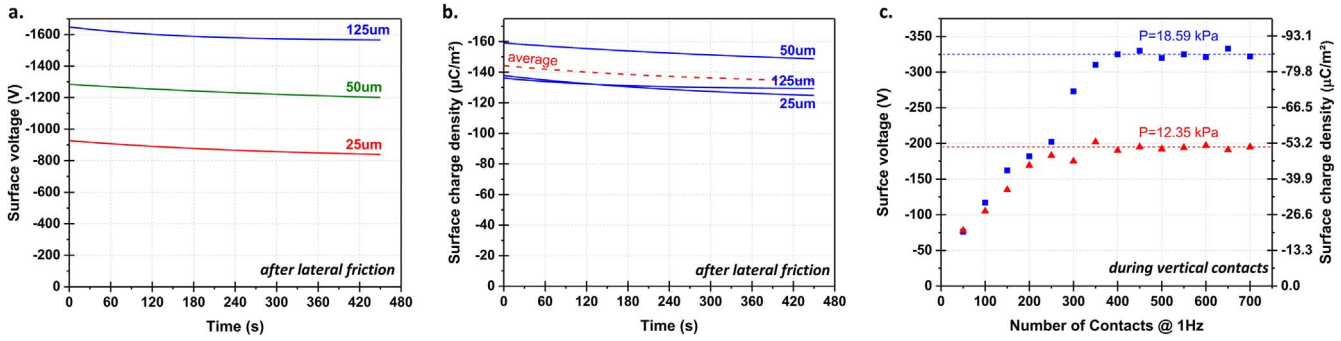

Fig. 4. Surface potential and charge density generated on PFA. a. Average curves of the exponential decay fitting of the surface potential and b. surface charge density generated by lateral friction of an Al top electrode on PFA films of various thickness attached with an adhesive tape of 100 μm on a bottom Al electrode. c. Evolution of the surface potential and surface charge density on a 50 μm PFA film attached with 20 μm of glue on a bottom Al electrode, as a function of the number of vertical contacts at 1 Hz with an Al top electrode and depending on the pressure applied.

triboelectric charge generation and saturation.

In a first set of experiments, we fabricated $2 \times 2\,cm^2$ T-ENGs using perfluoroalkoxy alkanes (PFA) films of various thickness. Before measurement, we make sure to deplete the charges on the surface of PFA films and we verified its very low surface potential using an electrostatic voltmeter. Then, we shortly rubbed multiple samples using Al electrodes and we recorded the surface potential decay with time. Then we averaged samples' results and we fitted the surface voltage decrease using an exponential decay ($y = y_0 + A_1 \times e^{(-x/t1)}$) (Fig. 4a). Finally, using the Eq. (3), we deduced the surface charge density generated on the PFA film (Fig. 4b). Overall, we observed that a similar friction, in terms of force, frequency and displacement, gives a similar surface charge density, leading to different surface potentials depending on the film thickness. The frictions saturate the surface of PFA films very quickly to a surface charge density varying from 130 to 155 $\mu C/m^2$. Once the friction stops, the surface charge slowly decreased. The fitting curves of the surface voltage decay showed that the surface voltage saturation level y_0 has little discrepancy with deviation percentages

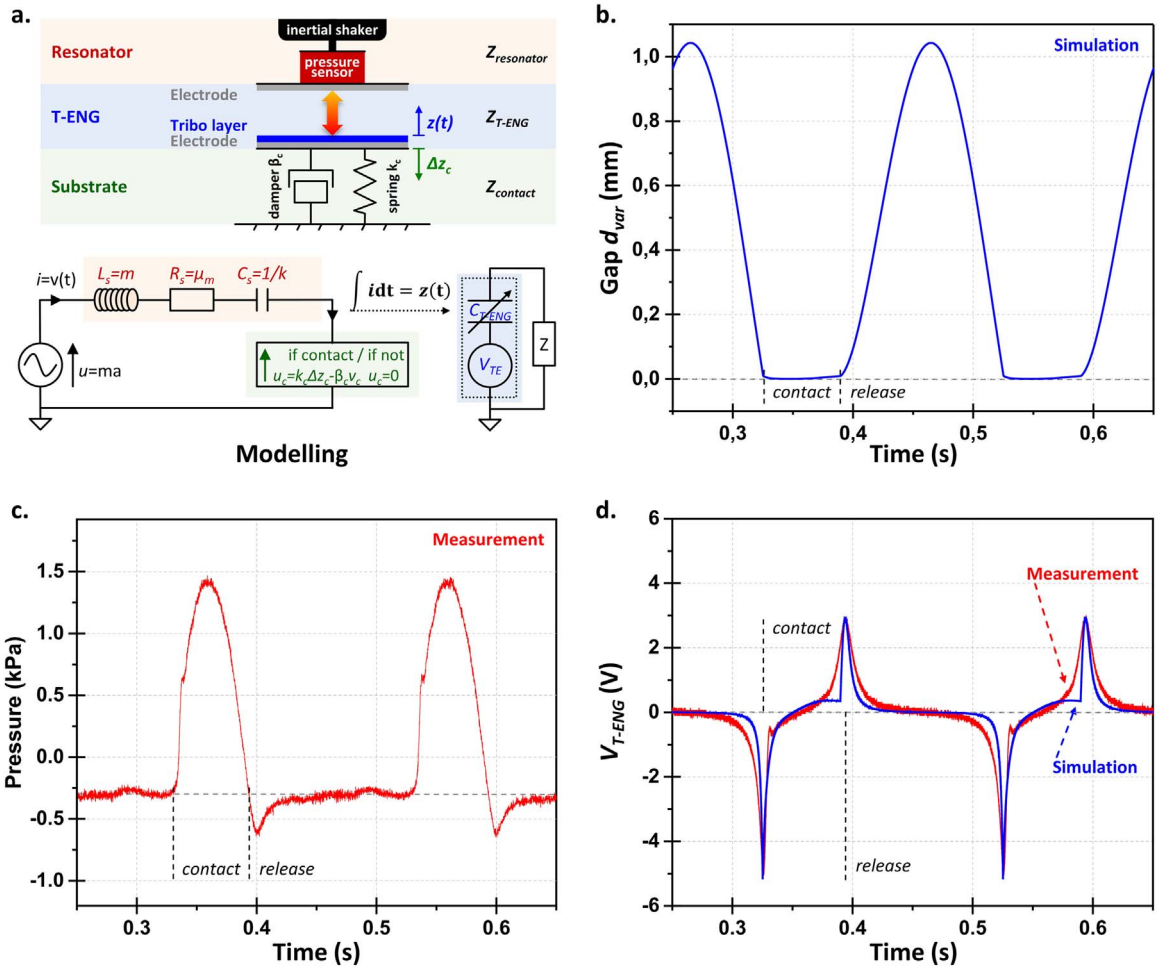

Fig. 5. Comparison between simulation and experimental results. a. The experimental T-ENG system is composed of a top Al electrode attached to an inertial shaker and a 50 μm PFA film attached on Al adhesive tape as bottom electrode with 20 μm of glue. The whole mechanical system including the resonator, triboelectret layer and substrate were electrically modeled. b. modeled displacement of the T-ENG top electrode. The spring constant used to simulate the contact was k' = 80,000 a.u. and the dumping was β = 200 a.u. c. measurement of the force applied on the T-ENG during its actuation. d. comparison between the voltage difference generated experimentally by the T-ENG through a load R_L = 10 MΩ with a parasitic capacitance of 2.5 pF and its electrical modeling.

between 5.62% and 11.6% depending on samples. However, we noted a high divergence concerning the decay amplitude A_1 and the time constant t_1 with deviation percentages up to 79.4%. First, these results indicate that the triboelectric friction generate charges at a consistent level. It is efficient and quickly saturates the surface of PFA films. Secondly, the behavior of the triboelectric charges has a very high variability. It is probably because they are mostly located on the surface, thereby exposed and sensitive to the ambient conditions. Indeed, the decay depends on numerous complex parameters (*e.g.* surface state, friction, humidity, temperature or light). However, the PFA layer's ability to trap and keep charges at a specific level is reliable.

To study the triboelectric charge generation dynamic, we performed multiple vertical contacts and followed the surface voltage evolution (Fig. 4c). In this case, the friction is much softer and the charge generation is lower. We found that the surface charge density increased with the number of contacts and saturated at different levels depending on the pressure applied during the contact, from 53 μC/m^2 under 12.35 kPa to 86.5 μC/m^2 under 18.59 kPa, which has a strong impact on the charge generation. The impact of the contact pressure on the surface charge density is due to the increase of the surface contact at micro scale between the triboelectric layer and the electrode when increasing the pressure. However, these hypothesis remain to be investigated. The precise nature of the triboelectric phenomenon is very complex, sensitive and still under investigation [45–50]. It depends on numerous conditions such as the humidity and the temperature, and parameters such as the surface state that we did not controlled precisely in this first approach.

To verify experimentally our model, we simulated and characterized a real triboelectric device and compared their results. This time, we fabricated a 3 cm × 3 cm T-ENG using 50 μm PFA film and Al tape (with 20 μm glue). The top electrode was attached to an inertial shaker (resonator) oscillating at a frequency of 5 Hz with an amplitude of about 2 mm. The device was placed at 1 mm of the shaker, parallel to the top electrode, in order to have a large movement and a good contact and we recorded the voltage generated through a load resistance of 10 MΩ for 5 s. Taking into account our measurement equipment, we estimated having a parasitic capacitance of 2.5 pF. For accurately simulating the real device, it is important to know very precisely its movement especially close to contact because we observed that most of the power is generated at less than 200 μm (Fig. 3d). To measure the top electrode displacement with sufficient accuracy, we first tried to use a laser. However, we could not get a high precision that meets the demand. We also tried to measure the acceleration of the top electrode and integrate it twice to calculate its displacement, but again it was not accurate enough. At last, we modeled the whole mechanical system including the inertial shaker (where a is its acceleration, m its mass, k its spring constant and μ_m its friction coefficient), the T-ENG and the elastic contact between the Al top electrode and the PFA triboelectric layer using a spring k_c and damping elements β_c (where z_c is the vertical contact displacement and v the contact speed) [51] (Fig. 5a).

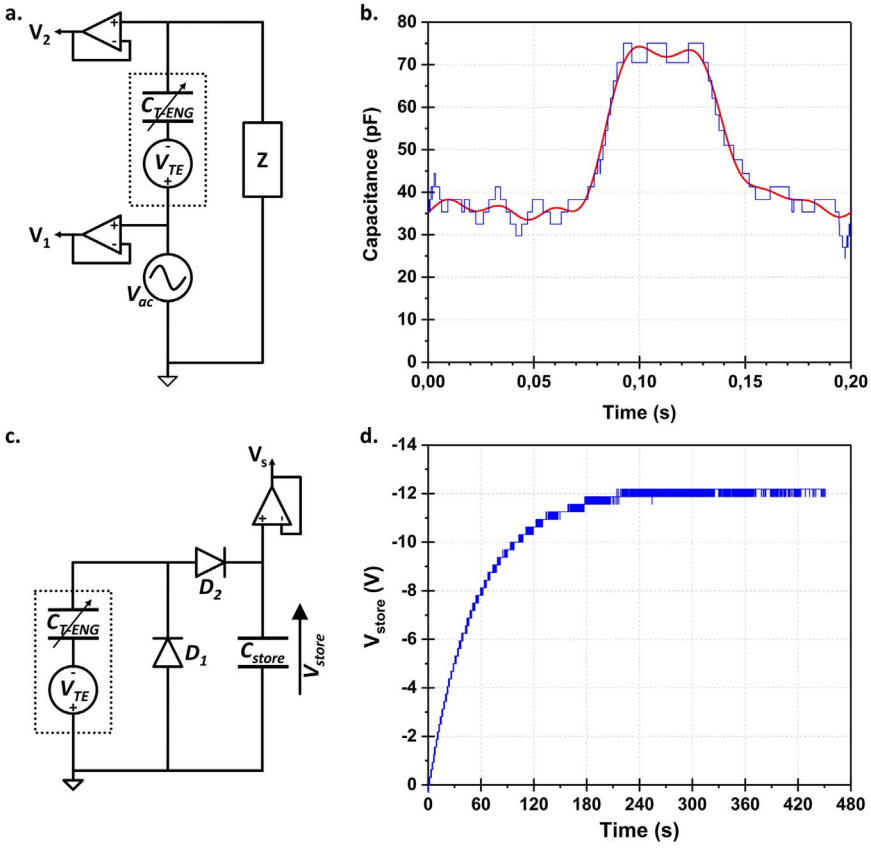

Fig. 6. Extraction of the electric model parameters. a. Electrical circuit for measuring and extracting the capacitance variation of the T-ENG [52]. b. Capacitance variation of the T-ENG depending on time. The parasitic capacitance of the setup is included in the measurement and reached 16 pF. The signal have been filtered with a low pass filter at 45 Hz. c. Electrical circuit for measuring the voltage source bias of the T-ENG [52]. d. T-ENG voltage store depending on time.

Considering a negligible mass for the top electrode, we electrically modeled the displacement and contact of the top electrode (Fig. 5b), and added it into the electrical model of the T-ENG. We also considered a surface charge density of 5 μC/m^2 that corresponds to a few touches under a low pressure of 1.5 kPa (Fig. 5c) according to previous measurements (Fig. 4c). Overall, the comparison between the experiment and the simulation agrees well (Fig. 5d). Both signals have very similar amplitude, and their peaks appear upon contact and release. The slight differences are mostly due to the difficulty in modeling the complex contact dynamics, as for the experimental setup, there are slight error in the parallel arrangement between electrodes and in the full contact of the layer despite their roughness.

Finally, to achieve a better simulation of a more complex and real T-ENG, we propose to measure its key parameters: its capacitance variation $C_{T\text{-}ENG}$ and its voltage bias V_{TE} (Fig. 1c). These parameters alone are sufficient to simulate a T-ENG, getting a good representation of its real performances and evaluating various conditioning circuit with a Spice simulator. Recently, several technics have been proposed to measure and extract these parameters for electret energy harvesters. To measure the capacitance variation $\Delta C_{T\text{-}ENG}$ of a T-ENG, different approaches are possible [51–54]. We followed the setup presented in [52] requiring a voltage source to measure the phase shift between two signals (Fig. 6a) and we found that the capacity of our TENG varied between 35 and 75 pF including all parasitic capacitances (Fig. 6b). The extracted maximum capacitance of the T-ENG C_{max} is lower than its theoretical value, which is normal and is in agreement with static measurements made using an LCR impedance meter. The parasitic capacitance was measured to be 16 pF using a known fixed capacitance. Similarly, to extract the voltage source bias V_{TE}, few methods have been proposed [52,55]. Here again we used a simple setup [52] (Fig. 6c) to extract the voltage source bias of our T-ENG that follows the Eq. (13):

$$V_{TE} = \frac{V_{Store}}{1 - C_{T-ENG\_min}/C_{T-ENG\_max}} \quad (13)$$

where C_{min} and C_{max} are the minimum and maximum capacitance of the T-ENG. Our prototype reached V_{TE} = 22.5 V (Fig. 6d). It is possible to estimate the quantity of charges generated at each cycle by multiplying the capacitance variation by the bias voltage. Likewise, the mechanical energy converted into electrical energy can be obtained by integrating the area surrounded by the *Q-V* cycle. In our case, each movement generated approximately 900 pC. Measuring $\Delta C_{T\text{-}ENG}$ and V_{TE} allow for truly comparing T-ENGs independently of working conditions such as the mechanical stimulus (*e.g.* frequency, speed) and measurement equipment (*e.g.* input impedance, parasitic capacitance). In addition, to compare performances, the RMS voltage and current as well as the average power generated should be prioritized, as they give a better picture of the full ability of the T-ENG.

6. Conclusions

In conclusion, we investigated the constitutive equations, the lumped model and the simulation of a planar T-ENG based on the extensive literature of electret energy harvesters, because T-ENGs follow the same electrical model than electret generators since they are both members of the family of electrostatic Kinetic Energy Harvester. We compared this electrical model to multiphysics FEM simulations and results were very close, with an error less than 3%. The model is composed of a variable capacitance and a voltage source. It can easily be introduced in a Spice simulator in order to develop conditioning circuits for the T-ENGs. The voltage source corresponds to the surface voltage of the triboelectric layer. We experimentally measured this surface voltage that a triboelectric PFA layer can reach when contacted with Al. It depends on a few parameters and is very sensitive to temperature and humidity conditions. Then we compared the T-ENG model to experimental results and found a good consistency. Finally, we proposed two setups to extract the electrical model parameters from real devices. These parameters are very useful to reconstitute and compare the performances of T-ENG. These results are very

encouraging. Such a T-ENG model has long been a key missing element for electronic engineers seeking to integrate T-ENG in electronic devices and use them to power industrial and consumer products. That is why it will be very useful for researchers who wish to compare and transfer T-ENG technologies. Thereby, it could greatly contribute the development and the expansion of the T-ENG.

Acknowledgments

This research was financially supported by the Center for Advanced Soft-Electronics as the Global Frontier Project (2013M3A6A5073177) and by the Technology Innovation Program(10065730, Flexible Power Module and System Development for Wearable Devices) funded by the Ministry of Trade, Industry & Energy (MOTIE, Korea).

Supporting information

Additional details include current, voltage and maximum power curves generated by the electrical model under various load resistances. The schematic of the T-ENG structure used in the FEM simulation and the gap, voltage and current curves results from the FEM simulation of the T-ENG. The surface voltage and surface charge density fitting curves measured on 125, 50 and 25 μm PFA film.

Appendix A. Supplementary material

Supplementary data associated with this article can be found in the online version at http://dx.doi.org/10.1016/j.nanoen.2018.02.030.

References

[1] O.D. Jefimenko, D.K. Walker, Electrostatic current generator having a disk electret as an active element, IEEE Trans. Ind. Appl. IA-14 (1978) 537–540, http://dx.doi.org/10.1109/TIA.1978.4503588.
[2] Y. Tada, Experimental characteristics of electret generator, using polymer film electrets, Jpn. J. Appl. Phys. 31 (1992) 846–851, http://dx.doi.org/10.1143/JJAP.31.846.
[3] G.M. Sessler, Electrets, Springer Berlin Heidelberg, Berlin, Heidelberg, 1987, http://dx.doi.org/10.1007/3-540-17335-8.
[4] F.-R. Fan, Z.-Q. Tian, Z. Lin Wang, Flexible triboelectric generator, Nano Energy 1 (2012) 328–334, http://dx.doi.org/10.1016/j.nanoen.2012.01.004.
[5] M. Eguchi, X.X. On, The permanent electret, Philos. Mag. Ser. 6 (49) (1925) 178–192, http://dx.doi.org/10.1080/14786442508634594.
[6] Y. Suzuki, Electrostatic/electret-based harvesters, in: D. Briand, E. Yeatman, S. Roundy (Eds.), Micro Energy Harvest, Wiley-VCH Verlag GmbH & Co. KGaA, Weinheim, Germany, 2015, pp. 149–174, , http://dx.doi.org/10.1002/9783527672943.ch8.
[7] P. Basset, E. Blokhina, D. Galayko, Electrostatic Kinetic Energy Harvesting, John Wiley & Sons, Inc., Hoboken, NJ, USA, 2016, http://dx.doi.org/10.1002/9781119007487.
[8] S. Boisseau, G. Despesse, B. Ahmed, Electrostatic conversion for vibration energy harvesting, in: M. Lallart (Ed.), Small-Scale Energy Harvest, InTech, 2012, p. 358, , http://dx.doi.org/10.5772/51360.
[9] G. Despesse, J.J. Chaillout, S. Boisseau, C. Jean-Mistral, Mechanical energy harvesting, Energy Autonomous Micro and Nano Systems, John Wiley & Sons, Inc, Hoboken, NJ, USA, 2013, pp. 115–151, , http://dx.doi.org/10.1002/9781118561836.ch5.
[10] K. Ikezaki, M. Miki, J. Tamura, Thermally stimulated currents from ion-injected Teflon-FEP film electrets, Jpn. J. Appl. Phys. 20 (1981) 1741–1747, http://dx.doi.org/10.1143/JJAP.20.1741.
[11] L.S. McCarty, A. Winkleman, G.M. Whitesides, Ionic electrets: electrostatic charging of surfaces by transferring mobile ions upon contact, J. Am. Chem. Soc. 129 (2007) 4075–4088, http://dx.doi.org/10.1021/ja067301e.
[12] Y. Lu, M. Capo-Chichi, Y. Leprince-Wang, P. Basset, A flexible electrostatic kinetic energy harvester based on electret films of electrospun nanofibers, Smart Mater. Struct. (2017), http://dx.doi.org/10.1088/1361-665X/aa87da.
[13] B. Gross, R.J. de Moraes, Polarization of the electret, J. Chem. Phys. 37 (1962) 710–713, http://dx.doi.org/10.1063/1.1733151.
[14] J.-H. Lee, R. Hinchet, T.Y. Kim, H. Ryu, W. Seung, H.-J. Yoon, S.-W. Kim, Control of skin potential by triboelectrification with ferroelectric polymers, Adv. Mater. 27 (2015) 5553–5558, http://dx.doi.org/10.1002/adma.201502463.
[15] T. Takamatsu, Life time of thermal electrets of carnauba wax, esters, fatty acids and alcohols, in: Proceedings of the 7th International Symposium on Electrets (ISE 7), IEEE, n.d.: 1991.: pp. 106–110. doi:10.1109/ISE.1991.167191.
[16] P. Bloß, M. Steffen, H. Schäfer, G.-M. Yang, G.M. Sessler, A comparison of space-charge distributions in electron-beam irradiated FEP obtained by using heat-wave and pressure-pulse techniques, J. Phys. D. Appl. Phys. 30 (1997) 1668–1675, http://dx.doi.org/10.1088/0022-3727/30/11/016.
[17] R. Gerhard-Multhaupt, M. Haardt, W. Eisenmenger, G.M. Sessler, Electric-field profiles in electron-beam-charged polymer electrets, J. Phys. D. Appl. Phys. 16 (1983) 2247–2256, http://dx.doi.org/10.1088/0022-3727/16/11/027.
[18] J.A. Giacometti, S. Fedosov, M.M. Costa, Corona charging of polymers: recent advances on constant current charging, Braz. J. Phys. 29 (1999) 269–279, http://dx.doi.org/10.1590/S0103-97331999000200009.
[19] P. Gunther, Mechanism of charge storage in electron-beam or corona-charged silicon-dioxide electrets, IEEE Trans. Electr. Insul. 26 (1991) 42–48, http://dx.doi.org/10.1109/14.68225.
[20] V.N. Kestelman, L.S. Pinchuk, V.A. Goldade, Electrets in Engineering, Springer, US, Boston, MA, 2000, http://dx.doi.org/10.1007/978-1-4615-4455-5.
[21] Y. Suzuki, Recent progress in MEMS electret generator for energy harvesting, IEEJ Trans. Electr. Electron. Eng. 6 (2011) 101–111, http://dx.doi.org/10.1002/tee.20631.
[22] C.B. Williams, R.B. Yates, Analysis of a micro-electric generator for microsystems, Sens. Actuators A Phys. 52 (1996) 8–11, http://dx.doi.org/10.1016/0924-4247(96)80118-X.
[23] T. Sterken, P. Fiorini, K. Baert, R. Puers, G. Borghs, An electret-based electrostatic?-generator, in: TRANSDUCERS '03. in: Proceedings of the 12th International Conference on Solid-State Sensors, Actuators Microsystems. Digital Technical Paper (Cat. No.03TH8664), IEEE: 2003: pp. 1291–1294. https://dx.doi.org/10.1109/SENSOR.2003.1217009〉.
[24] Hsi-wen Lo, Rus Whang, Yu-Chong Tai, A simple micro electret power generator, in: Proceedings of the IEEE 20th International Conference on Micro Electro Mechanical System, IEEE: 2007: pp. 859–862. 〈https://dx.doi.org/10.1109/MEMSYS.2007.4433004〉.
[25] J. Boland, Yuan-Heng Chao, Y. Suzuki, Y.C. Tai, Micro electret power generator, in: Proceedings of Sixth Annual International Conference on Micro Electro Mechanical System MEMS-03 Kyoto. IEEE, IEEE, n.d.: 2003.: pp. 538–541. doi:10.1109/MEMSYS.2003.1189805.
[26] G.M. Sessler, Charge distribution and transport in polymers, IEEE Trans. Dielectr. Electr. Insul. 4 (1997) 614–628, http://dx.doi.org/10.1109/94.625648.
[27] S. Niu, Y.S. Zhou, S. Wang, Y. Liu, L. Lin, Y. Bando, Z.L. Wang, Simulation method for optimizing the performance of an integrated triboelectric nanogenerator energy harvesting system, Nano Energy 8 (2014) 150–156, http://dx.doi.org/10.1016/j.nanoen.2014.05.018.
[28] S. Niu, Z.L. Wang, Theoretical systems of triboelectric nanogenerators, Nano Energy 14 (2015) 161–192, http://dx.doi.org/10.1016/j.nanoen.2014.11.034.
[29] S. Niu, S. Wang, L. Lin, Y. Liu, Y.S. Zhou, Y. Hu, Z.L. Wang, Theoretical study of contact-mode triboelectric nanogenerators as an effective power source, Energy Environ. Sci. 6 (2013) 3576, http://dx.doi.org/10.1039/c3ee42571a.
[30] E. Blokhina, D. Galayko, P. Basset, O. Feely, Steady-state oscillations in resonant electrostatic vibration energy harvesters, IEEE Trans. Circuits Syst. I Regul. Pap. 60 (2013) 875–884, http://dx.doi.org/10.1109/TCSI.2012.2209295.
[31] D. Galayko, P. Basset, A general analytical tool for the design of Vibration Energy Harvesters (VEHs) based on the mechanical impedance concept, IEEE Trans. Circuits Syst. I Regul. Pap. 58 (2011) 299–311, http://dx.doi.org/10.1109/TCSI.2010.2072030.
[32] D. Galayko, E. Blokhina, P. Basset, F. Cottone, A. Dudka, E. O'Riordan, O. Feely, Tools for analytical and numerical analysis of electrostatic vibration energy harvesters: application to a continuous mode conditioning circuit, J. Phys. Conf. Ser. 476 (2013) 12076, http://dx.doi.org/10.1088/1742-6596/476/1/012076.
[33] I.L. Baginsky, E.G. Kostsov, A.A. Sokolov, Electrostatic microgenerators of energy with a high specific power, Optoelectron. Instrum. Data Process. 46 (2010) 580–592, http://dx.doi.org/10.3103/S8756699011060100.
[34] P.D. Mitcheson, T.C. Green, E.M. Yeatman, A.S. Holmes, Architectures for vibration-driven micropower generators, J. Microelectromech. Syst. 13 (2004) 429–440, http://dx.doi.org/10.1109/JMEMS.2004.830151.
[35] C.C. Nguyen, D.C. Ranasinghe, S.F. Al-Sarawi, Analytical modeling and optimization of electret-based microgenerators under sinusoidal excitations, Microsyst. Technol. (2017), http://dx.doi.org/10.1007/s00542-017-3349-1.
[36] S. Chauhan, B. Müller, U. Mescheder, Simulation, fabrication and characterization of robust vibrational energy harvester, Procedia Eng. 120 (2015) 349–354, http://dx.doi.org/10.1016/j.proeng.2015.08.633.
[37] S. Boisseau, G. Despesse, T. Ricart, E. Defay, A. Sylvestre, Cantilever-based electret energy harvesters, Smart Mater. Struct. 20 (2011) 105013, http://dx.doi.org/10.1088/0964-1726/20/10/105013.
[38] K.R.G. P.D. Mitcheson, T.C. Green, Mixed electromechanical simulation of electrostatic microgenerator using custom-semiconductor device models, Proc. Power. (2009) 356–359.
[39] D. Galayko, K. Caluwaerts, P. Basset, Modelling techniques for capacitive harvesters of vibration energy, Proc. PowerMEMS (2008) 445–448.
[40] S. Niu, S. Wang, Y. Liu, Y.S. Zhou, L. Lin, Y. Hu, K.C. Pradel, Z.L. Wang, A theoretical study of grating structured triboelectric nanogenerators, Energy Environ. Sci. 7 (2014) 2339, http://dx.doi.org/10.1039/c4ee00498a.
[41] S. Meninger, J.O. Mur-Miranda, R. Amirtharajah, A. Chandrakasan, J.H. Lang, Vibration-to-electric energy conversion, IEEE Trans. Very Large Scale Integr. Syst. 9 (2001) 64–76, http://dx.doi.org/10.1109/92.920820.
[42] Y. Zi, S. Niu, J. Wang, Z. Wen, W. Tang, Z.L. Wang, Standards and figure-of-merits for quantifying the performance of triboelectric nanogenerators, Nat. Commun. 6 (2015) 8376, http://dx.doi.org/10.1038/ncomms9376.
[43] S. Roundy, P.K. Wright, J. Rabaey, A study of low level vibrations as a power source for wireless sensor nodes, Comput. Commun. 26 (2003) 1131–1144, http://dx.doi.org/10.1016/S0140-3664(02)00248-7.

[44] K. Dai, X. Wang, S. Niu, F. Yi, Y. Yin, L. Chen, Y. Zhang, Z. You, Simulation and structure optimization of triboelectric nanogenerators considering the effects of parasitic capacitance, Nano Res. 10 (2017) 157–171, http://dx.doi.org/10.1007/s12274-016-1275-7.
[45] L.S. McCarty, G.M. Whitesides, Electrostatic charging due to separation of ions at interfaces: contact electrification of ionic electrets, Angew. Chem. Int. Ed. Engl. 47 (2008) 2188–2207, http://dx.doi.org/10.1002/anie.200701812.
[46] D.J. Lacks, R. Mohan Sankaran, Contact electrification of insulating materials, J. Phys. D. Appl. Phys. 44 (2011) 453001, http://dx.doi.org/10.1088/0022-3727/44/45/453001.
[47] F. Galembeck, T.A.L. Burgo, L.B.S. Balestrin, R.F. Gouveia, C.A. Silva, A. Galembeck, Friction, tribochemistry and triboelectricity: recent progress and perspectives, RSC Adv. 4 (2014) 64280–64298, http://dx.doi.org/10.1039/C4RA09604E.
[48] L. Beraldo da Silveira Balestrin, D. Del Duque, D. Soares da Silva, F. Galembeck, Triboelectricity in insulating polymers: evidence for a mechanochemical mechanism, Faraday Discuss. 170 (2014) 369–383, http://dx.doi.org/10.1039/C3FD00118K.
[49] M.W. Williams, Triboelectric charging of insulators - evidence for electrons versus ions, in: Proceedings of IEEE Industry Applications Society Annual Meeting, IEEE, 2010: pp. 1–6. doi:10.1109/IAS.2010.5615666.
[50] M.W. Williams, Triboelectric charging of insulating polymers–some new perspectives, AIP Adv. 2 (2012) 10701, http://dx.doi.org/10.1063/1.3687233.
[51] P. Basset, D. Galayko, A.M. Paracha, F. Marty, A. Dudka, T. Bourouina, A batch-fabricated and electret-free silicon electrostatic vibration energy harvester, J. Micromech. Microeng. 19 (2009) 115025, http://dx.doi.org/10.1088/0960-1317/19/11/115025.
[52] Y. Lu, E. O'Riordan, F. Cottone, S. Boisseau, D. Galayko, E. Blokhina, F. Marty, P. Basset, A batch-fabricated electret-biased wideband MEMS vibration energy harvester with frequency-up conversion behavior powering a UHF wireless sensor node, J. Micromech. Microeng. 26 (2016) 124004, http://dx.doi.org/10.1088/0960-1317/26/12/124004.
[53] J. Oxaal, D. Foster, M. Hella, D.-A. Borca-Tasciuc, Investigation of gap-closing interdigitated capacitors for electrostatic vibration energy harvesting, J. Micromech. Microeng. 25 (2015) 105010, http://dx.doi.org/10.1088/0960-1317/25/10/105010.
[54] A. Karami, D. Galayko, P. Basset, Characterization of the capacitance variation of electrostatic vibration energy harvesters biased following rectangular charge-voltage diagrams, J. Phys. Conf. Ser. 773 (2016) 12015, http://dx.doi.org/10.1088/1742-6596/773/1/012015.
[55] A. Karami, D. Galayko, P. Basset, A. Novel, Characterization method for accurate lumped parameter modeling of electret electrostatic vibration energy harvesters, IEEE Electron Device Lett. 38 (2017) 665–668, http://dx.doi.org/10.1109/LED.2017.2682232.

Dr. Ronan Hinchet is a postdoctoral researcher in the School of Advanced Materials Science and Engineering at Sungkyunkwan University (SKKU). He received his PhD degree from the University of Grenoble in Nanoelectronics and Nanotechnology in 2014. His research interests are the simulation, fabrication, and characterization of nanostructures and nanomaterials for micro-electro-mechanical system and nano-electro-mechanical system applications. His research is focused on mechanical energy harvesters and mechanical sensor applications.

Ali Ghaffarinejad is pursuing his Ph.D. degree in electrical engineering at School of Electrical Engineering, Iran University of Science and Technology (IUST), Tehran, Iran. He received his B.Sc. degree in electronics engineering from the University of Kerman, Iran, in 2006, the M.Sc. degree in Biomedical engineering from IUST in 2011. He is currently a visiting student at ESYCOM lab, Université Paris-Est/ESIEE, Paris, France. His research interests include study of triboelectric charge transfer and induction through rough surfaces, design and modeling of RF-MEMS devices. He focus on the modeling and characterization of triboelectric transducers and interface circuits for mechanical energy harvesters.

Yingxian Lu is a PhD student under the co-supervision of Professor Philippe Basset and Jean-Marc Laheurte at ESYCOM lab, Université Paris-Est. Her research interests include kinetic energy harvesters for power supply applications of wireless sensor nodes or for wearable electronics, MEMS device modeling, design and characterization, RF system optimization, and flexible electronic devices. Her research is focused on capacitive kinetic energy harvesters working with ultra-low frequency vibrations or motions, including random environmental vibrations, machine vibrations, or human motions.

Dr. Javad Yavand Hasani is a professor in the School of Electrical Engineering at Iran University of Science and Technology (IUST), Tehran, Iran. In 2009 he received the PhD degree in electrical engineering from the University of Tehran and the PhD degree in high frequency and optics from the University of Joseph Fourier (UJF), Grenoble, France. From 2012–2014 he was the dean of the Electronic Research Center (ERC) in IUST. His current research interests include high frequency circuits and systems, as well as micro-fabrication theory and technology for RF and microwave devices, MEMS and NEMS.

Dr. Sang-Woo Kim is professor in School of Advanced Materials Science and Engineering at Sungkyunkwan University (SKKU). He received his Ph.D. from Kyoto University, Department of Electronic Science and Engineering in 2004. After working as postdoctoral researcher at Kyoto University and University of Cambridge, he spent 4 years as assistant professor at Kumoh National Institute of Technology. He joined the SKKU in 2009. His research is focused on piezoelectric/triboelectric nanogenerators, photovoltaics, and 2D nanomaterials. Now he is the Associate Editor of Nano Energy and an Executive Board Member of Advanced Electronic Materials.

Dr. Philippe Basset is professor at Université Paris-Est / ESIEE Paris. He received his Ph.D from IEMN / University of Lille in 2003 in the areas of microelectronic and microelectro-mechanical-systems (MEMS). In 2004 he was a postdoc at CMU, Pittsburgh, USA and he joined ESIEE Paris in 2005. His current research interests include micro-power sources for autonomous MEMS and micro/nano-structuration of silicon. He serves in the International Steering Committee of the PowerMEMS conference since 2015. Member of the ESYCOM laboratory, he is currently leading the Sensors and Measuring MEMS group.